



US008559685B2

(12) **United States Patent**
Rivaz et al.

(10) **Patent No.:** **US 8,559,685 B2**
(45) **Date of Patent:** **Oct. 15, 2013**

(54) **ROBUST AND ACCURATE FREEHAND 3D ULTRASOUND**

(56) **References Cited**

(75) Inventors: **Hassan Rivaz**, Baltimore, MD (US);
Emad Moussa Bector, Baltimore, MD (US);
Gabor Fichtinger, Kingston (CA);
Gregory Hager, Baltimore, MD (US)

(73) Assignee: **The Johns Hopkins University**,
Baltimore, MD (US)

(*) Notice: Subject to any disclaimer, the term of this patent is extended or adjusted under 35 U.S.C. 154(b) by 771 days.

(21) Appl. No.: **12/449,582**

(22) PCT Filed: **Feb. 19, 2008**

(86) PCT No.: **PCT/US2008/002116**

§ 371 (c)(1),
(2), (4) Date: **Apr. 7, 2010**

(87) PCT Pub. No.: **WO2008/100623**

PCT Pub. Date: **Aug. 21, 2008**

(65) **Prior Publication Data**

US 2010/0198068 A1 Aug. 5, 2010

Related U.S. Application Data

(60) Provisional application No. 60/901,873, filed on Feb. 16, 2007.

(51) **Int. Cl.**
G06K 9/00 (2006.01)

(52) **U.S. Cl.**
USPC **382/128**

(58) **Field of Classification Search**
None
See application file for complete search history.

U.S. PATENT DOCUMENTS

7,901,357 B2 *	3/2011	Bector et al.	600/443
2002/0120195 A1 *	8/2002	Hossack et al.	600/443
2003/0018442 A1	1/2003	Yamaguchi et al.	
2005/0101865 A1	5/2005	Hao et al.	
2005/0187473 A1 *	8/2005	Bector et al.	600/437
2006/0229744 A1	10/2006	Patzwald et al.	
2010/0198068 A1 *	8/2010	Rivaz et al.	600/443

OTHER PUBLICATIONS

A. H. Gee, R. J. Housden, P. Hassenpflug, G. M. Treece, and R. W. Prager. Sensorless freehand 3D ultrasound in real tissue: speckle decorrelation without fully developed speckle. *Medical Image Analysis*, Jan. 2005, pp. 1-19.*
Housden et al., Sub-sample Interpolation Strategies for Sensorless Freehand 3D Ultrasound, *Ultrasound Med. Biology* Jan. 2006, vol. 32(12); 1897-904.*

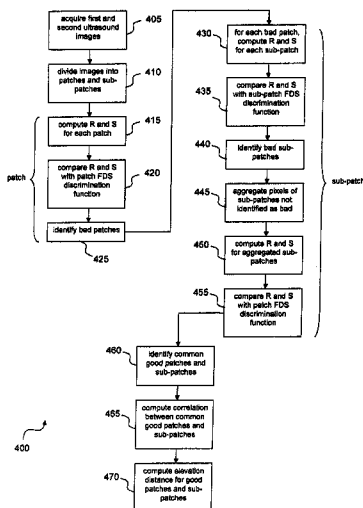
(Continued)

Primary Examiner — Bhavesh Mehta
Assistant Examiner — Tahmina Ansari
(74) *Attorney, Agent, or Firm* — Venable LLP; Henry J. Daley

(57) **ABSTRACT**

Disclosed is a system and method for computing out of plane motion between two ultrasound images. The method identifies regions of fully developed speckle that are common to the two images, computes a correlation coefficient corresponding to the two fully developed speckle image regions, and then computing an elevation distance corresponding to the correlation coefficient. The method exploits the measurable and characterizable relation between inter-image correlation and elevation distance, which may be determined from fully developed speckle regions. The method also identifies regions within the ultrasound images related to structure (e.g., vein or bone), and disregards these regions.

20 Claims, 13 Drawing Sheets



(56)

References Cited

OTHER PUBLICATIONS

Rivaz, H. et al., "Real-Time Regularized Ultrasound Elastography" Medical Imaging, IEEE Transactions on vol. 30, Issue: 4 Publication Year: 2011, pp. 928-945 Digital Object Identifier: 10.1109/TMI.2010.2091966.*

Azar, A.A. et al. "Speckle detection in ultrasonic images using unsupervised clustering techniques", Engineering in Medicine and Biol-

ogy Society,EMBC, 2011 Annual International Conference of the IEEE, Publication Year: 2011 , pp. 8098-8101, Digital Object Identifier: 10.1109/IEMBS.2011.6091997.*

Housden et al., "Sub-sample Interpolation Strategies for Sensorless Freehand 3D Ultrasound," Ultrasound Med. Biol 2006, vol. 32(12); 1897-904, Retrived from the Internet Jul. 3, 2008, http://mi.eng.cam.ac.uk/reports/svr-ftp/housden_tr545.pdf, pp. 1-11.

* cited by examiner

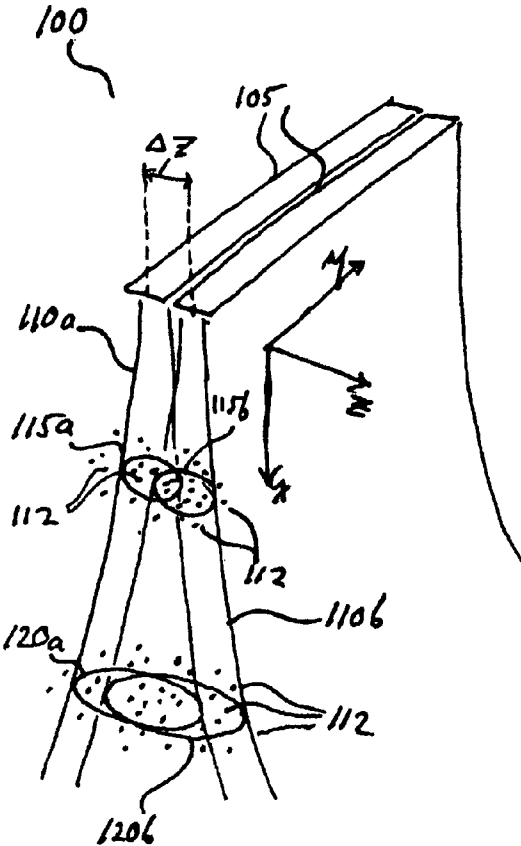


FIG. 1A

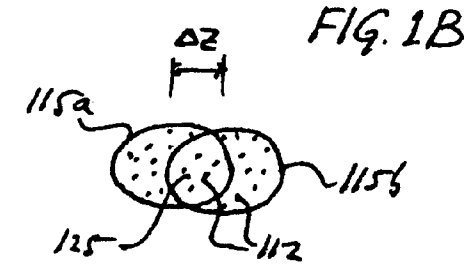


FIG. 1B

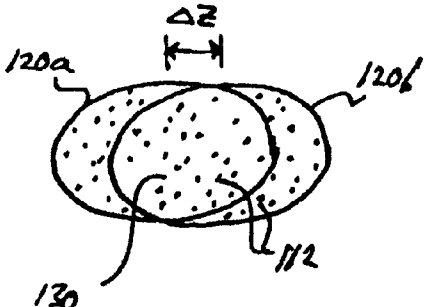


FIG. 1C

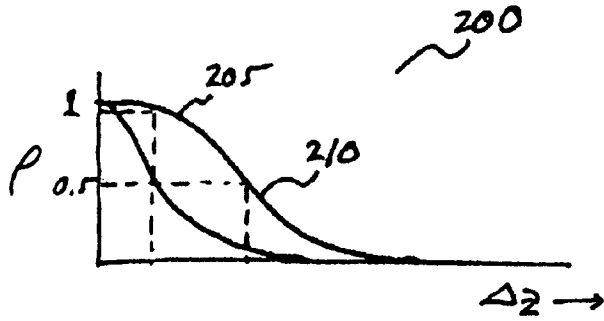


FIG. 2

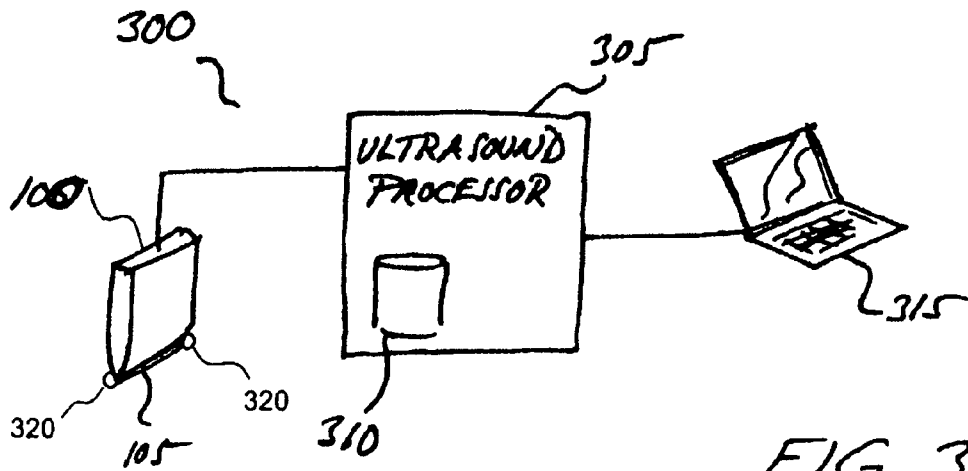
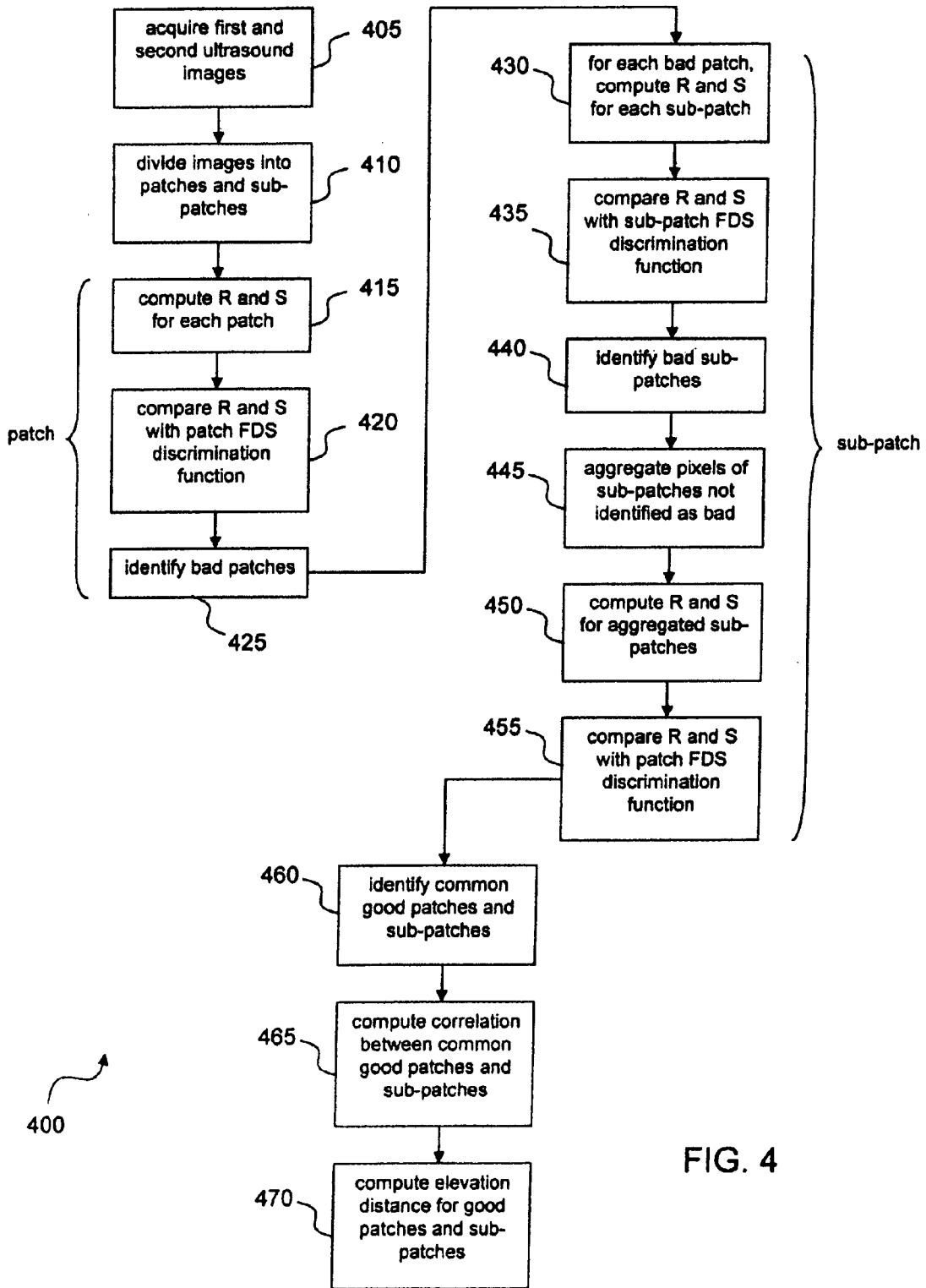


FIG. 3



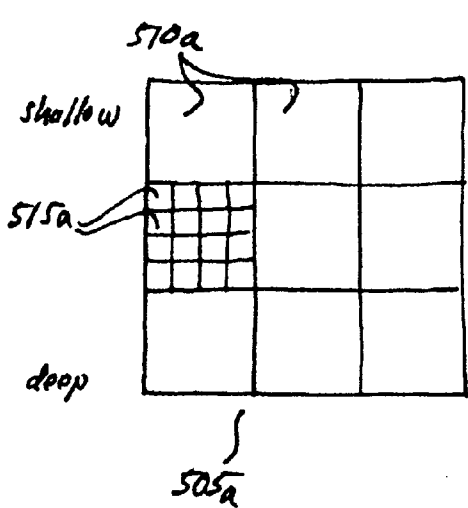


FIG. 5A

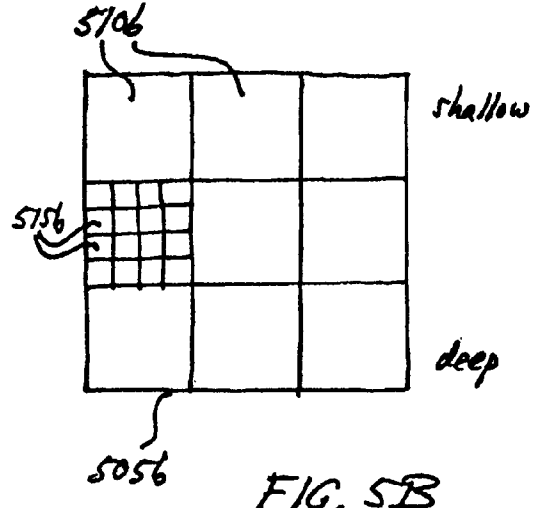


FIG. 5B

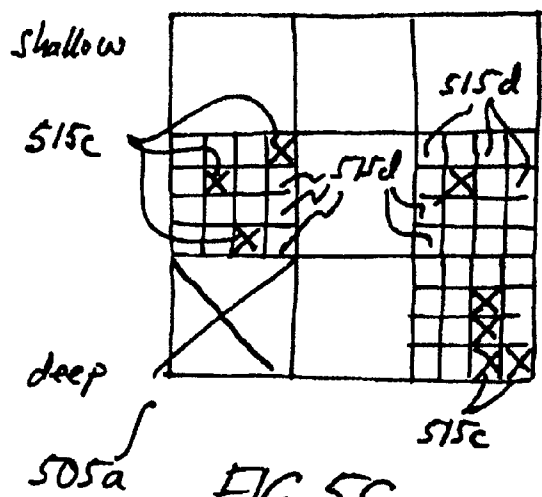
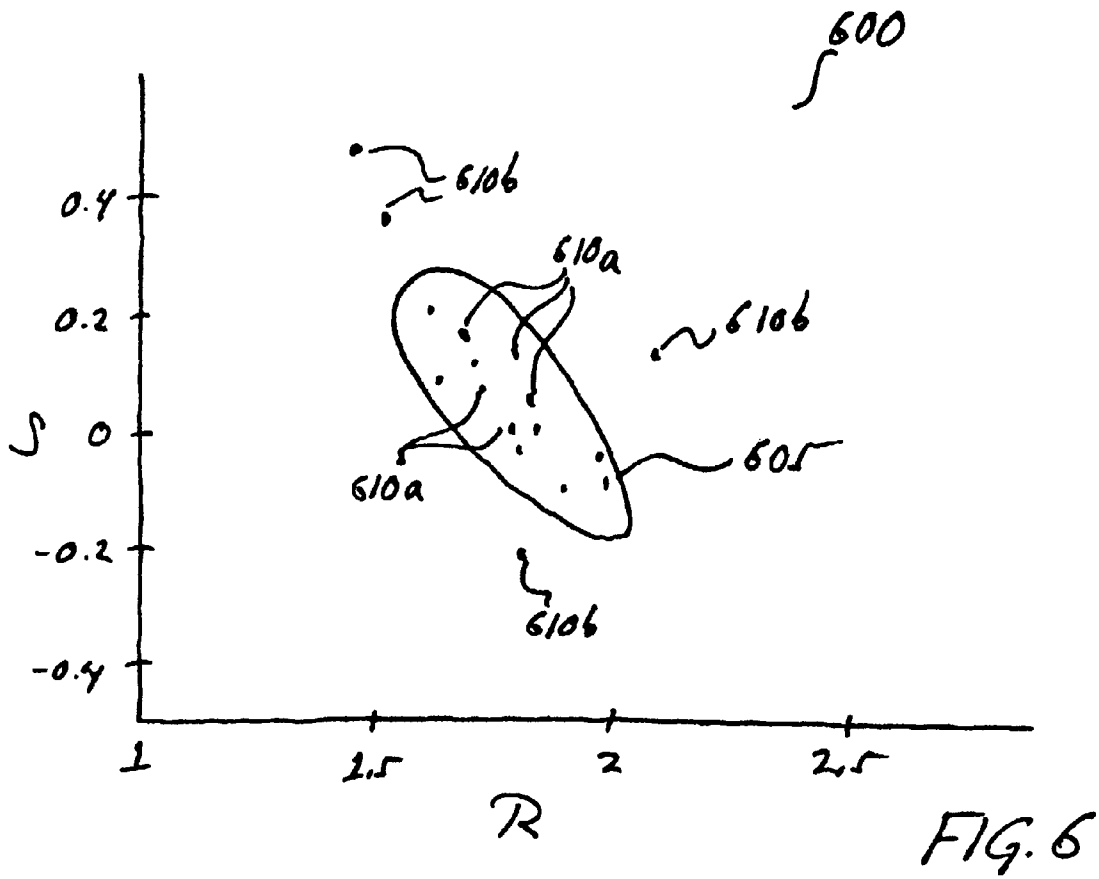


FIG. 5C



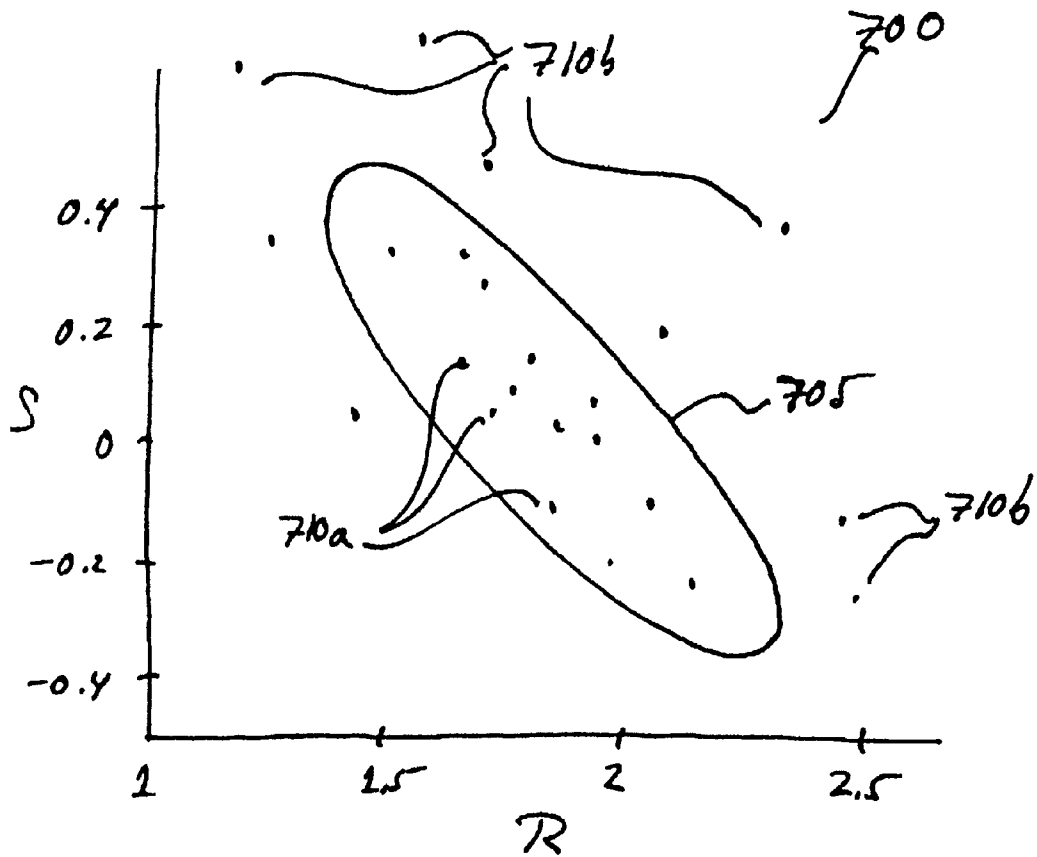
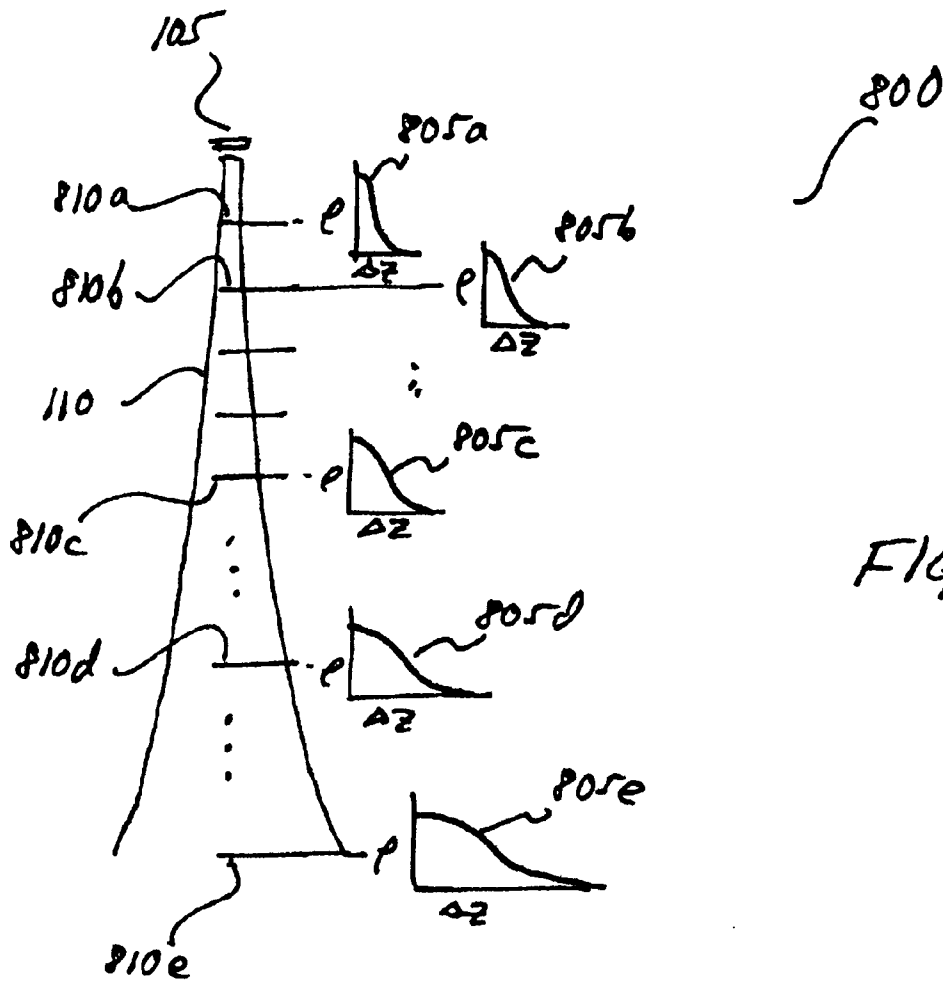


FIG. 7



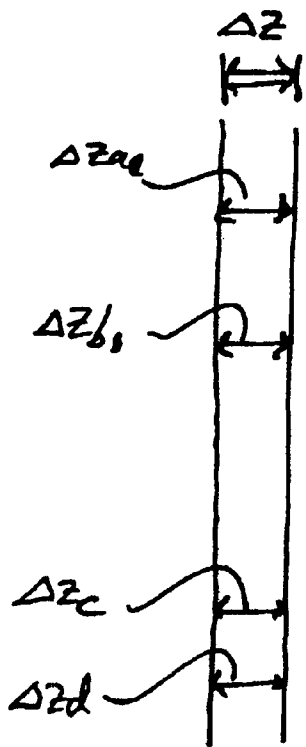


FIG. 9A

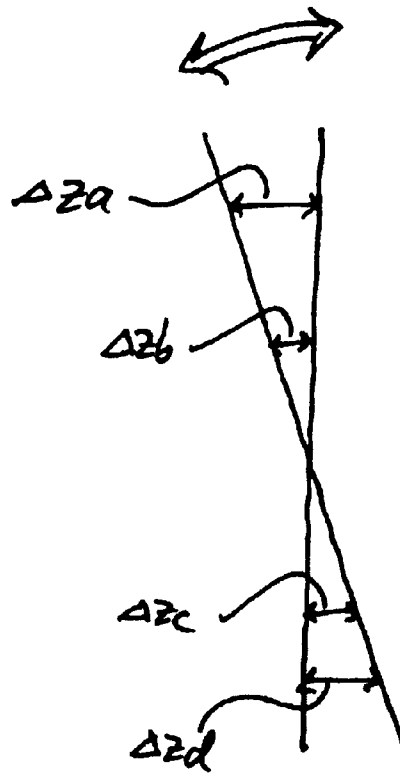


FIG. 9B

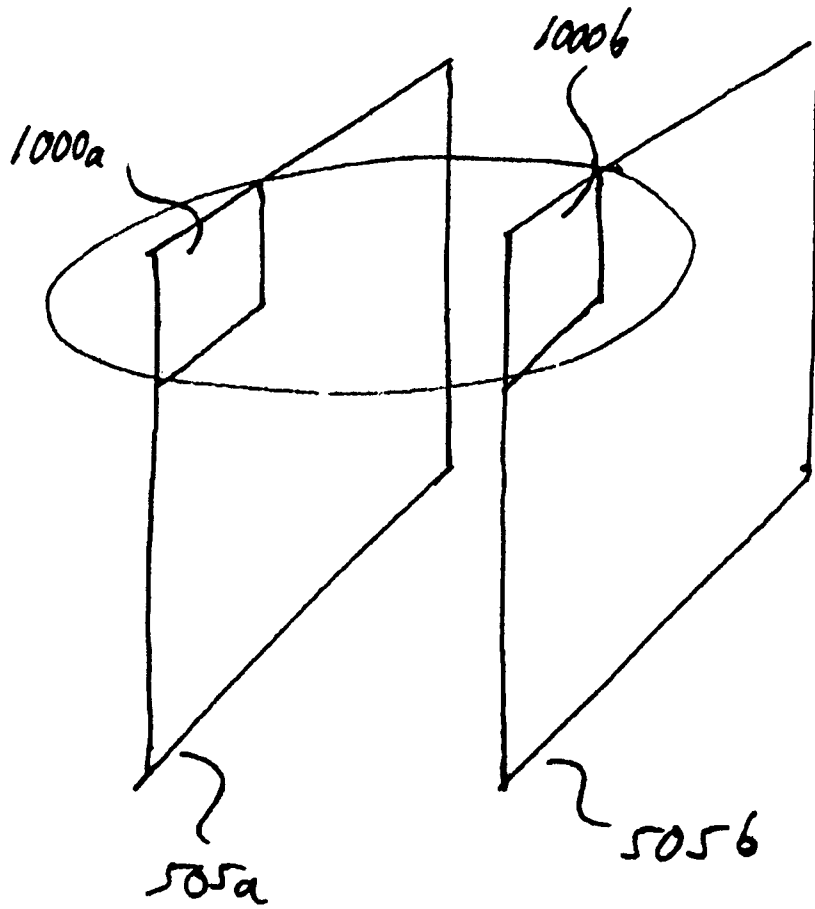


FIG. 10

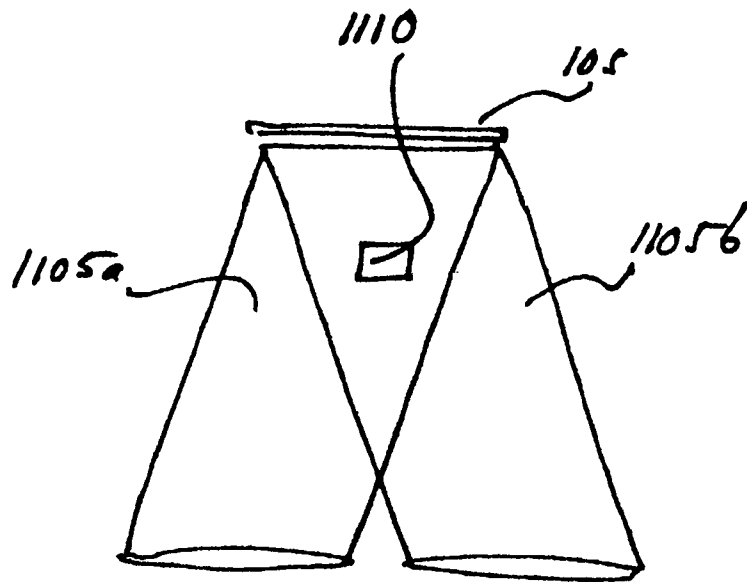


FIG. 11

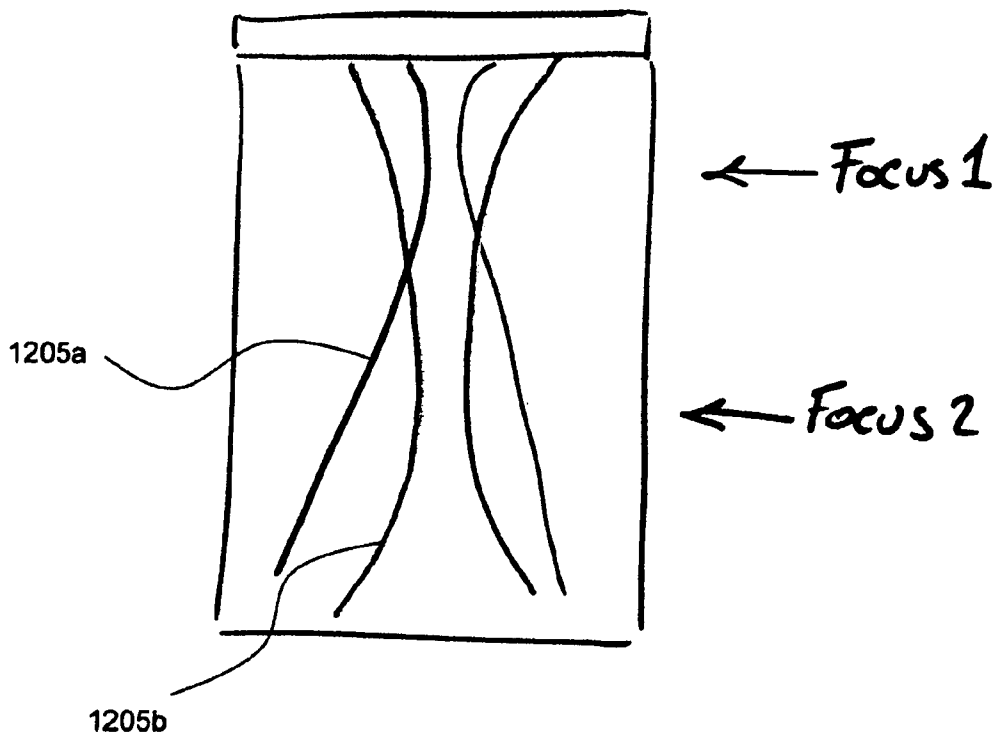


FIG. 12

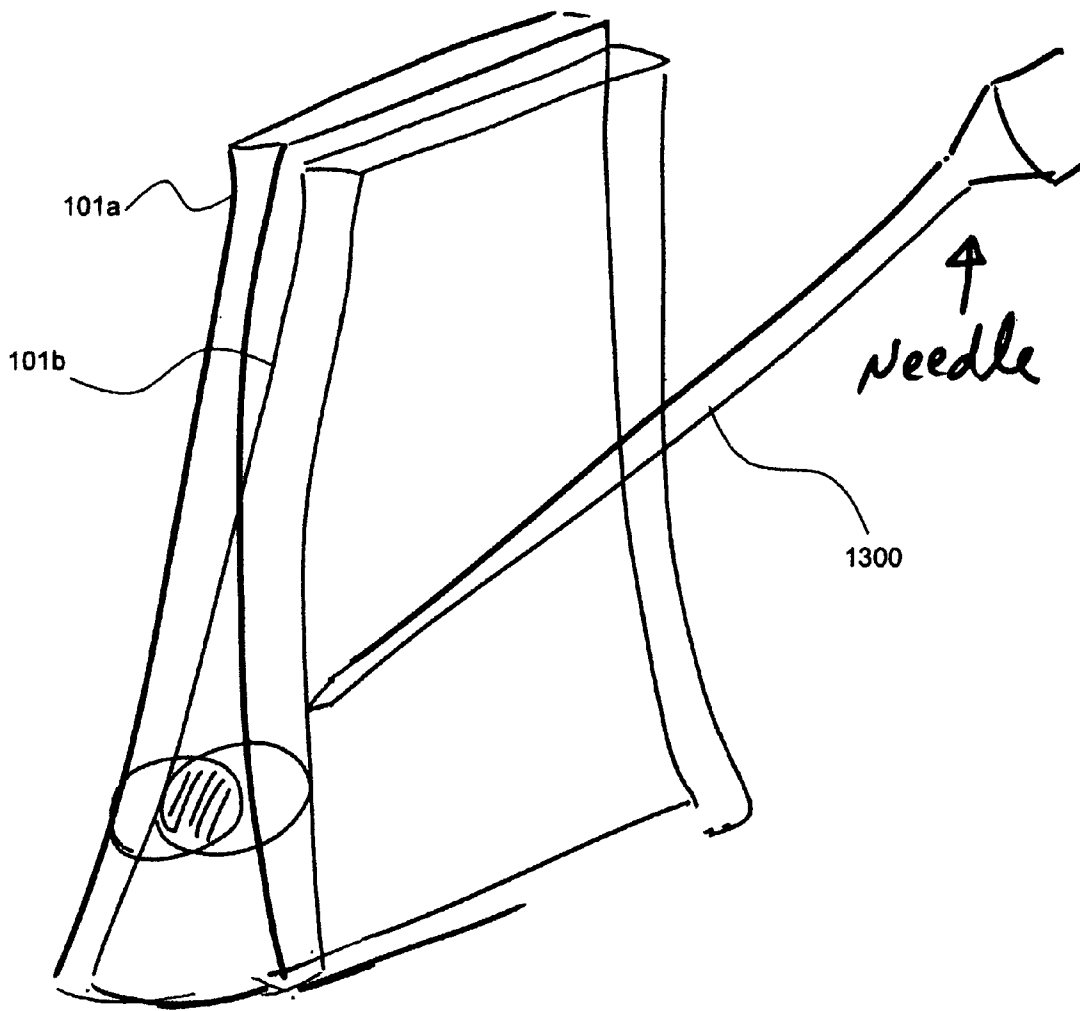


FIG. 13

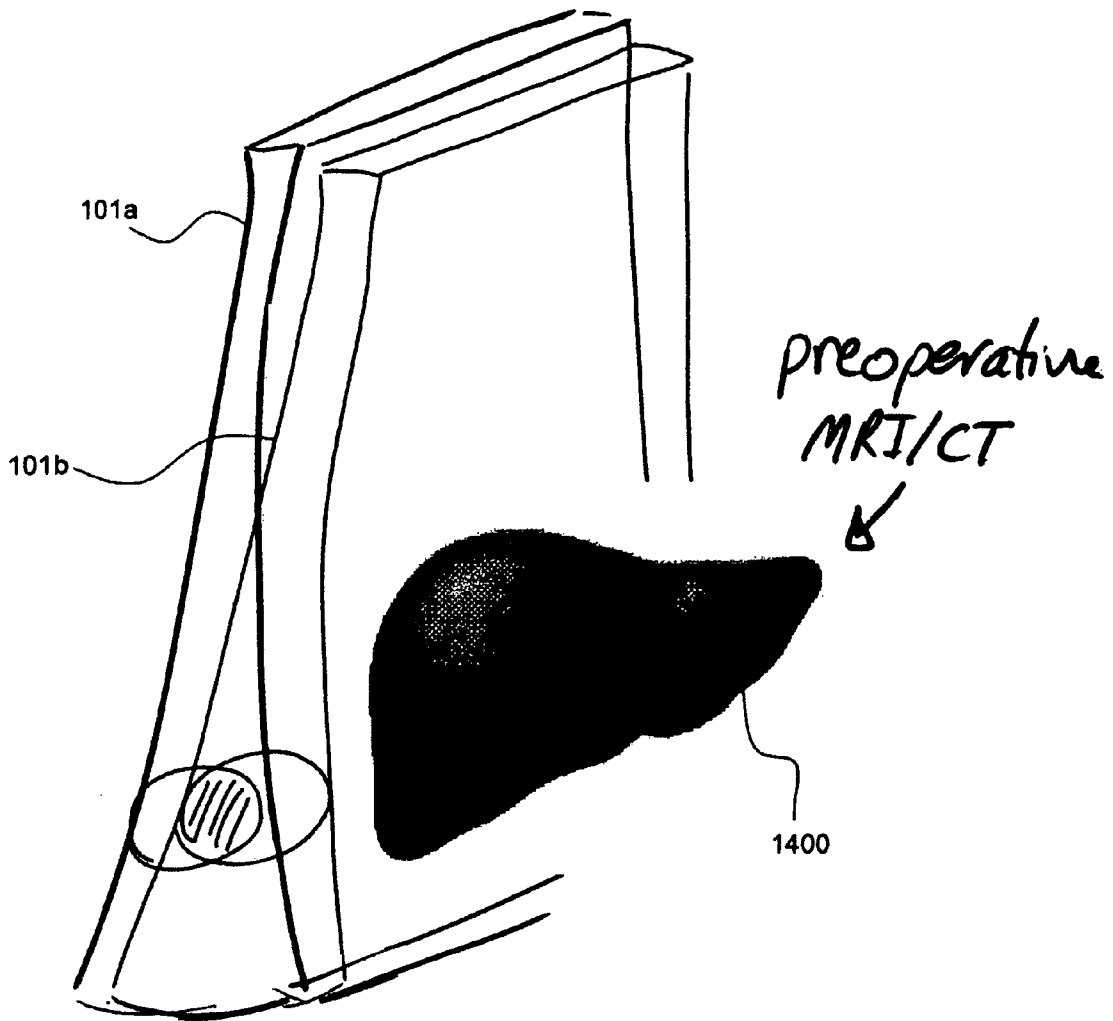


FIG. 14

ROBUST AND ACCURATE FREEHAND 3D ULTRASOUND

This application claims the benefit of PCT Application No. PCT/US2008/002116, filed on Feb. 19, 2008 and U.S. Provisional Patent Application No. 60/901,873, filed on Feb. 16, 2007, which is hereby incorporated by reference for all purposes as if fully set forth herein.

BACKGROUND

1. Field of the Invention

The present invention generally relates to ultrasound imaging. More particularly, the application relates to the generation of 3D images using ultrasound.

2. Discussion of the Related Art

Ultrasound imaging has become a widely used medical imaging modality, due in part to its effectiveness in safely imaging tissue, its ease of use, and lower cost. Ultrasound has become an essential imaging tool in applications such as identifying tissue anomalies, monitoring fetal development, and assisting in guiding surgical devices in invasive treatments.

Considerable effort has recently been devoted to generating 3D images from multiple ultrasound images. By acquiring multiple images of a tissue region of interest, from multiple angles and positions, it is possible to merge the multiple images to generate a 3D image. Approaches to accomplishing this have included (a) precisely measuring the position and orientation of the ultrasound probe for each image acquired; and/or (b) identifying common tissue features across multiple images to serve as markers for registering the plurality of images into a single 3D image space.

Precisely measuring the position and orientation of the ultrasound probe generally requires additional equipment, which is expensive, and complicates the use of the ultrasound probe. For example, one related art approach involves attaching the ultrasound probe to a robotic arm, which precisely controls the position and orientation of the ultrasound probe. Another related art approach involves mounting optical tracking devices to a handheld ultrasound probe. The latter approach requires equipping the room with optical scanning devices, which is expensive to implement and restricts the use of the ultrasound probe to the room in which the optical scanning devices are installed. Further, line-of-sight between the optical scanning devices and the optical tracking devices (mounted on the ultrasound probe) must be maintained in order for the position and orientation of the ultrasound probe to be computed. Both of these related art solutions add considerable cost and complexity to an ultrasound system.

As mentioned above, another approach involves identifying tissue features common to multiple images for registering multiple ultrasound images to a single 3D image space. This is typically done by inferring the relative position and orientation of the ultrasound probe by determining the location of the common tissue features in each ultrasound image. This is generally easier if the ultrasound probe's motion is constrained to the ultrasound image plane, so that the same common features appear in each ultrasound image. In this case, it is generally easy to compute the translation and rotation of the ultrasound probe by computing the displacement of the tissue features between images. However, this is not so simple in the case of out of plane motion. Out of plane motion is that in which the ultrasound probe translates and/or rotates so that tissue features move with a vector component perpendicular to the ultrasound image plane. In this case, tissue features,

which are typically required to register one image to another, disappear due to motion of the ultrasound probe.

Accordingly, what is needed is a system and method for registering multiple ultrasound images into a single 3D image space, without the expense and complication of additional control/measurement hardware, and which addresses the problem of out of plane motion.

SUMMARY OF THE INVENTION

The present invention provides a method for robust and accurate 3D ultrasound that obviates one or more of the aforementioned problems due to the limitations of the related art.

Accordingly, one advantage of the present invention is that it improves ultrasound probe calibration for 3D ultrasound imaging.

Another advantage of the present invention is that it provides for more robust ultrasound image registration.

Another advantage of the present invention is that it better provides for ultrasound image-guided surgical interventions.

Still another advantage of the present invention is that it improves out of plane motion tracking of ultrasound speckle features.

Additional advantages of the invention will be set forth in the description that follows, and in part will be apparent from the description, or may be learned by practice of the invention. The advantages of the invention will be realized and attained by the structure pointed out in the written description and claims hereof as well as the appended drawings

To achieve these and other advantages, the present invention involves a method for generating 3D ultrasound imagery. The method comprises acquiring a first ultrasound image and a second ultrasound image, the first ultrasound image corresponding to a first image location, and second ultrasound image corresponding to a second image location, and wherein the first image location and the second image location are separated by an elevation distance; dividing the first ultrasound image and the second ultrasound image into a plurality of patches; computing a signal to noise ratio value and a skewness value for each of the plurality of patches; comparing the signal to noise ratio value and skewness value for each patch to a range of acceptable signal to noise ratio values and a range of acceptable skewness values; determining if there is a plurality of good patches, wherein the good patches have a corresponding signal to noise ratio value and skewness value that lie within the range of acceptable signal to noise ratio values and skewness values; if it is determined that there is a plurality of good patches, computing a correlation coefficient for a corresponding pair of good patches, wherein one of the corresponding pair is from the first ultrasound image, and the other of the corresponding pair is from the second ultrasound image; if it is determined that there is a plurality of good patches, computing an elevation distance corresponding to the correlation coefficient; and constructing a 3D image using the first and second ultrasound images and the elevation distance.

In another aspect of the present invention, the aforementioned and other advantages are achieved by a method for determining out of plane motion between a first ultrasound image and a second ultrasound image, which comprises dividing the first ultrasound image into a first plurality of patches, wherein each of the first plurality of patches has a first plurality of pixel data; dividing the second ultrasound image into a second plurality of patches, wherein each of the second plurality of patches has a second plurality of pixel data; combining one of the first plurality of pixel data with a

corresponding one of the second pixel data; computing a signal to noise ratio value and a skewness value corresponding to the combined pixel data; comparing the signal to noise ratio value and skewness value with a range of acceptable signal to noise ratio values and skewness values; depending on a result of the comparing, computing a correlation coefficient corresponding to the one of one of the first plurality of pixel data with the corresponding one of the second pixel data; computing an elevation distance corresponding to the correlation coefficient and constructing a 3D image using the first ultrasound image, the second ultrasound image, and the elevation distance.

In another aspect of the present invention, the aforementioned and other advantages are achieved by a system for generating 3D ultrasound images. The system comprises an ultrasound probe; a processor coupled to the ultrasound probe; and a memory coupled to the processor, wherein the memory is encoded with instructions for acquiring a first ultrasound image and a second ultrasound image, the first ultrasound image corresponding to a first image location, and second ultrasound image corresponding to a second image location, and wherein the first image location and the second image location are separated by an elevation distance; dividing the first ultrasound image and the second ultrasound image into a plurality of patches; computing a signal to noise ratio value and a skewness value for each of the plurality of patches; comparing the signal to noise ratio value and skewness value for each patch to a range of acceptable signal to noise ratio values and a range of acceptable skewness values; determining if there is a plurality of good patches, wherein the good patches have a corresponding signal to noise ratio value and skewness value that lie within the range of acceptable signal to noise ratio values and skewness values; if it is determined that there is a plurality of good patches, computing a correlation coefficient for a corresponding pair of good patches, wherein one of the corresponding pair is from the first ultrasound image, and the other of the corresponding pair is from the second ultrasound image; and if it is determined that there is a plurality of good patches, computing an elevation distance corresponding to the correlation coefficient.

In yet another aspect of the present invention, the aforementioned and other advantages are achieved by a system for generating 3D ultrasound images. The system comprises an ultrasound probe; a processor coupled to the ultrasound probe; and a memory coupled to the processor, wherein the memory is encoded with instructions for acquiring a first ultrasound image and a second ultrasound image; dividing the first ultrasound image into a first plurality of patches, wherein each of the first plurality of patches has a first plurality of pixel data; dividing the second ultrasound image into a second plurality of patches, wherein each of the second plurality of patches has a second plurality of pixel data; combining one of the first plurality of pixel data with a corresponding one of the second pixel data; computing a signal to noise ratio value and a skewness value corresponding to the combined pixel data; comparing the signal to noise ratio value and skewness value with a range of acceptable signal to noise ratio values and skewness values; depending on a result of the comparing, computing a correlation coefficient corresponding to the one of one of the first plurality of pixel data with the corresponding one of the second pixel data; computing an elevation distance corresponding to the correlation coefficient, and constructing a 3D image using the first ultrasound image, the second ultrasound image, and the elevation distance.

It is to be understood that both the foregoing general description and the following detailed description are exem-

plary and explanatory and are intended to provide further explanation of the invention as claimed.

BRIEF DESCRIPTION OF THE DRAWINGS

The accompanying drawings, which are included to provide a further understanding of the invention and are incorporated in and constitute a part of this specification, illustrate embodiments of the invention and together with the description serve to explain the principles of the invention.

FIG. 1A illustrates two exemplary ultrasound probe fields of view, in which the fields of view are separated by an out of plane motion;

FIG. 1B illustrates two overlapping resolution cells that are relatively close to the ultrasound probe, or in a shallow region of the tissue medium;

FIG. 1C illustrates two overlapping resolution cells that are relatively far from the ultrasound probe, or in a deep region of the tissue medium;

FIG. 2 illustrates an exemplary correlation curve set;

FIG. 3 illustrates an exemplary system for freehand ultrasound 3D imaging;

FIG. 4 illustrates an exemplary process for freehand ultrasound 3D imaging;

FIG. 5A illustrates an exemplary first ultrasound image, which is divided into patches and sub-patches;

FIG. 5B illustrates an exemplary second ultrasound image, which is divided into patches and sub-patches;

FIG. 5C illustrates an exemplary first ultrasound image, in which bad sub-patches are identified and tagged;

FIG. 6 illustrates an exemplary skewness vs. signal to noise plot corresponding to the patches of FIGS. 5A and 5B;

FIG. 7 illustrates an exemplary skewness vs. signal to noise plot corresponding to the sub-patches of FIG. 5C;

FIG. 8 illustrates an exemplary ultrasound field of view, along with exemplary image depths;

FIG. 9A illustrates an exemplary out of plane translation between two fields of view;

FIG. 9B illustrates an exemplary out of plane rotation between two fields of view;

FIG. 10 illustrates an two corresponding patches, each of a different ultrasound image, which are merged into a single patch;

FIG. 11 illustrates two beamsteered ultrasound fields of view and a patch that is imaged by both of these fields of view;

FIG. 12 illustrates two ultrasound fields of view that are acquired using different focusing modes;

FIG. 13 illustrates two ultrasound fields of view imaging a structure of known shape, wherein the structure is a surgical device; and

FIG. 14 illustrates two ultrasound fields of view imaging a structure of known shape, wherein the structure is a previously-imaged anatomical feature.

DETAILED DESCRIPTION

The system and method described herein exploits the traits of Fully Developed Speckle (FDS) in ultrasound imagers, whereby the extent of correlation between two images of a single FDS feature falls off at a measurable and characterizable rate as a function of out of plane distance, and as a function of depth within the ultrasound image.

FIG. 1A illustrates an ultrasound probe **100** acquiring two successive images while being scanned in an out of plane direction. Probe **100** has a transducer array **105**, which is depicted at two sequential scan positions. Transducer array **105** has a first field of view **110a**, corresponding to a first scan

position, and a second field of view **110b**, corresponding to a second scan position. First field of view **110a** has a shallow resolution cell **115a** and a deep resolution cell **120a**. Shallow resolution cell **115a** is a volume within field of view **110a** that corresponds to the field of view of a single transducer for a given sample integration time. The timing of the sample integration time is such that shallow resolution cell **115a** is a specific distance from transducer array **105**, which is closer to transducer array **105** than deep resolution cell **120a**. Deep resolution cell **120a** has a volume defined by the field of view of the same transducer as **115a**, but a sample integration time such that the sample is acquired further from transducer array **105**, i.e., deeper into the tissue than shallow resolution cell **115a**.

FIG. 1A also illustrates an ultrasound image coordinate space, having an axial direction (x-axis), a lateral direction (y-axis), and an elevation direction (z-axis, also referred to the out of plane direction). As illustrated, second field of view **110b** is offset from first field of view **110a** by a translation (Δz , also referred to as “elevation distance”) along the elevation direction, or z-axis. Further, as illustrated, both fields of view **110a** and **110b** have substantially similar geometry such that the y and z dimensions of the resolution cells within a given field of view increase as a function of distance along the x direction.

Further although FIG. 1A only illustrates resolution cells at two different depths (deep and shallow), one skilled in the art will readily recognize that these resolution cells are examples of a plurality of resolution cells that propagate along the x direction, such that the y and z dimensions of a resolution cell may be dictated by the geometry of transducer array **105**, the acoustic properties of the tissue medium, and the distance along the x axis, and that the x dimension of a given resolution cell is a function of the sample integration time employed by ultrasound probe **100**.

FIG. 1A further illustrates a plurality of speckle scatterers **112** that are distributed throughout the tissue medium. As illustrated, speckle scatterers **112** are distributed throughout the shallow resolution cells **115a** and **115b**, and deep resolution cells **120a** and **120b**.

FIG. 1B illustrates shallow resolutions cells **115a** and **115b**, as viewed along the x axis. Shallow resolution cells **115a** and **115b** have an overlap region **125**, the area of which is determined by the areas of shallow resolution cells **115a** and **115b**, and elevation distance Δz . Further illustrated are speckle scatterers **112**, distributed throughout shallow resolution cells **115a** and **115b**, including overlap region **125**.

FIG. 1C illustrates deep resolution cells **120a** and **120b**, as viewed along the x axis. Deep resolution cells **120a** and **120b** have an overlap region **130**, the area of which is determined by the areas of deep resolution cells **120a** and **120b**, and elevation distance Δz . Further illustrated are speckle scatterers **112**, distributed throughout deep resolution cells **120a** and **120b**, including overlap region **130**.

As illustrated in FIGS. 1B and 1C, the ratio of the area of overlap region **130** to the area of deep resolution cell **120a** or **120b** is greater than the ratio of the area of overlap region **125** to the area of shallow resolution cell **115a** or **115b**. This is due to the fact that the area of a resolution cell within an ultrasound field of view gets larger as a function of distance along the axial or x direction, and that the elevation distance Δz remains substantially constant (given that fields of view **110a** and **110b** are spatially offset by a translation with little or no rotation).

Given the increase in overlap region in proportion to resolution cell area as a function of axial distance, a higher percentage of speckle scatterers **112** are common to deep reso-

lution cells **120a** and **120b**, as compared to shallow resolution cells **115a** and **115b**. The result of this is that, in imaging a substantially uniform tissue medium, there will be a higher correlation in ultrasound signals between two deep resolution cells **120a** and **120b**, relative to shallow resolution cells **115a** and **115b**. Further, that the correlation between ultrasound signals for shallow and deep resolution cells **115a/115b** and **120a/120b** diminishes as a function of elevation distance Δz .

FIG. 2 illustrates an exemplary correlation curve set **200** for two resolution cells corresponding to two different tissue depths. Correlation curve **205** corresponds the correlation between two shallow resolution cells **115a** and **115b**, as a function of elevation distance Δz . And correlation curve **210** corresponds to the correlation between two deep resolution cells **120a** and **120b**, as a function of elevation distance Δz . As illustrated, for both curves **205** and **210**, given a substantially isotropic tissue medium, with a distribution of a sufficient number of speckle scatterers **112**, the correlation coefficient ρ may behave as a function of elevation distance Δz according to a Rayleigh distribution. In order for correlation curve **205** or **210** to have a Rayleigh distribution, there must be at least 10 speckle scatterers **112** within overlap region **125** and **130**.

As used herein, Fully Developed Speckle (FDS) may refer to a density and distribution of speckle scatterers **112** such that there are at least 10 speckle scatterers **112** within overlapping regions of corresponding resolution cells.

As illustrated in FIG. 2, a correlation ρ of 0.5 (for example), corresponds to a greater elevation distance Δz for deeper resolution cells than for shallower resolution cells. Conversely, for a given elevation distance Δz , the correlation ρ is greater for deeper resolution cells than for shallower resolution cells. Accordingly, if one knows the depth (along the axial or x direction) of a given resolution cell, and if one can compute a correlation between two overlapping resolution cells at that depth, one may use correlation curve set **200** to determine the elevation distance Δz between corresponding resolution cells of two fields of view.

However, this is generally difficult because tissue medium is rarely isotropic within two fields of view, such as first field of view **110a** and second field of view **110b**. The presence of structure within the tissue medium, such as veins, bone, and the like, create correlations between overlapping resolution cells that do not diminish as a function of elevation distance Δz , as is the case with FDS. In other words, the persistent correlation induced by structure within a tissue interferes with the ability to exploit FDS to determine elevation distance Δz as a function of correlation.

FIG. 3 illustrates an exemplary system **300** for generating 3D ultrasound images. System **300** may include an ultrasound probe **100**, and ultrasound processor **305** having a memory device **310**, and a user interface **315**. All of the components of system **300** may be parts of an existing commercial ultrasound system, with memory device **310** having additional machine readable instructions for performing processes disclosed herein. Alternatively, ultrasound processor **305** may be a separate computer or computer system, which receives ultrasound image data from a separate standalone ultrasound system.

Further, system **300** may also include one or more additional motion sensors **320**. Additional motion sensors **320** may include, for example, an optical tracking device similar to the LED or image correlation-based tracking used in a computer mouse. In this example, additional sensors **320** (optical tracking devices) may be placed on either side of transducer array **105**. As an ultrasound technician moves ultrasound probe **100** over a patient’s anatomy, the optical tracking devices detect the direction and displacement over

the patient's skin. By using two optical tracking sensors, additional two degree of freedom motion information between first field of view **110a** and **110b** may be obtained. Ultrasound processor **305** may execute instructions to acquire the motion data from the optical tracking sensors, compute a two degree of freedom solution for motion between fields of view **110a** and **110b**, and store this information in memory **310**. Alternatively (or additionally) additional sensors **320** may include other types of motion sensors, such as accelerometers, and the like. One skilled in the art will readily appreciate that such variations to additional sensors **320** (and to system **300**) are possible and within the scope of the invention.

Memory device **310** may include one or more computer readable storage media. Memory device **310** may include multiple storage devices that are accesses over a network. One skilled in the art will readily appreciate that many variations to system **300** are possible and within the scope of the invention.

FIG. **4** illustrates an exemplary process **400** for generating 3D ultrasound images. Process **400** may be performed by the processor(s) within system **300**. All of the processes disclosed herein may be implemented as machine readable instructions, stored in memory **310**. Alternatively, all or some of the processes disclosed herein may be stored in one or more memory devices that are part of a computer system that is separate from ultrasound imaging system **300**. In the latter case, additional processing hardware may be added to existing ultrasound imaging system **300** to enhance its processing capability for performing processes disclosed herein. One skilled in the art will readily recognize that such variations are possible and within the scope of the invention.

At step **405**, ultrasound processor **305** executes instructions to acquire a first ultrasound image and a second ultrasound image from ultrasound probe **100**. Ultrasound probe **100** is moved between these image acquisitions—or is moving during these image acquisitions—so that the first ultrasound image corresponds to first field of view **110a**, and the second ultrasound image corresponds to second field of view **110b**, which are separated by elevation distance Δz . Ultrasound processor **305** then stores the first and second ultrasound images in memory **310**. The desired elevation distance Δz may be such that shallow resolution cells **115a** and **115b** have sufficient overlap so that their computed correlation coefficient ρ is approximately 0.5. This is because, at lower correlation coefficient ρ values, the error in elevation distance Δz as a function of correlation coefficient ρ value becomes severe. This will be apparent to one skilled in the art by observing the shape of the correlation curve set **200** of FIG. **2**.

At step **410**, ultrasound processor **305** executes instructions to divide the first and second ultrasound images into patches, wherein each patch is an aggregate of a predetermined number of pixels in a predetermined geometry.

FIG. **5A** illustrates an exemplary first ultrasound image **505a**, corresponding to first field of view **110a**; and FIG. **5B** illustrates an exemplary second ultrasound image **505b**, corresponding to second field of view **110b**. First and second ultrasound images **505a** and **505b** are each composed of a plurality of pixels (not shown). Each pixel column (for both images) corresponds to a transducer within transducer array **105**. Each row of pixels is corresponds to a sample time, as processed by ultrasound probe **100**.

As illustrated in FIGS. **5A** and **5B**, first ultrasound image **505a** and second ultrasound image **505b** are respectively divided into a plurality of sub-patches **510a** and **510b**, in accordance with step **410**. Each patch **510a** and **510b** may have, for example, around 4000-5000 pixels, arranged in a

square or rectangular geometry. Other pixel quantities are possible. The number of patches, and the number of pixels per patch, may vary, with a tradeoff between processing time and expected anisotropy of the tissue, as well as other factors.

Further to step **410**, ultrasound processor **305** may execute instructions to divide each patch **510a** and **510b** into a plurality of sub-patches **515a** and **515b**. Each patch **510a** and **510b** may be divided into, for example, 18 columns and 7 rows of sub-patches **515a** and **515b**, respectively. Further, each sub-patch **515a** and **515b** may encompass, for example, around 700 pixels. One skilled in the art will readily appreciate that this configuration is exemplary, and other arrangements and geometries of sub-patches **515a** and **515b** are possible and within the scope of the invention.

Still further to step **410**, ultrasound processor **305** may execute instructions to normalize first ultrasound image **505a** by dividing the amplitude of each pixel by the mean amplitude of all of the pixels of first ultrasound image **505a**. The same may be done for second ultrasound image **505b**.

At step **415**, ultrasound processor **305** executes instructions to compute the signal-to-noise ratio and skewness (hereinafter referred to collectively as “R and S”) of each patch **505a** and **505b**. In doing so, ultrasound processor **305** may execute instructions to compute R and S according to the following relations:

$$R = \frac{\langle A^{v_r} \rangle}{\sqrt{\langle A^{2v_r} \rangle - \langle A^{v_r} \rangle^2}} \equiv \frac{\text{mean}}{\text{variance}}$$

$$S = \frac{\langle (A^{v_s} - \langle A^{v_s} \rangle)^3 \rangle}{(\langle A^{2v_s} \rangle - \langle A^{v_s} \rangle^2)^{3/2}} \equiv \frac{\text{skew}}{\text{variance}}$$

where A is the amplitude of the ultrasound RF envelope within patch **505a** or **505b**, v_r and v_s are signal powers, and $\langle \dots \rangle$ denotes the mean. Signal powers may be set so that $v_r = 2v_s = 1$, as an example. Accordingly, ultrasound processor **305** executes instructions to compute R and S for each patch **505a** and **505b**, and stores the corresponding values in memory **310**.

At step **420**, ultrasound processor **305** executes instructions to compare the R and S values for each patch **505a** and **505b** with an FDS discrimination function.

FIG. **6** illustrates a skewness vs. signal to noise plot (hereinafter S/R plot) **600**, which graphically depicts the FDS discrimination function. Also depicted is an FDS patch ellipse **605**. FDS patch ellipse **605** is a predetermined R and S parameter space that may graphically plot as an ellipse on S/R plot **600**. FDS patch ellipse **605** defines a boundary, or range, of acceptable R and S values, so that R and S values within the FDS patch ellipse correspond to a patch that has speckle scatterers **112** of sufficient quantity and distribution to result in a symmetric Gaussian distribution. In other words, the statistical qualities of the speckle scatterers within a given patch have a sufficient signal to noise ratio and skewness to provide a correlation coefficient ρ of sufficient fidelity to provide an elevation distance Δz between first field of view **110a** and second field of view **110b**. In other words, R and S values **610a** are to be considered FDS (fully developed speckle), which may be used to calculate elevation distance Δz (i.e., out of plane motion distance). R and S values **610b** that lie outside FDS patch ellipse **605** correspond to patches have either an insufficient number of speckle scatterers **112**, or that have some structure (e.g., vein or bone), which contaminates the statistical properties of the pixel amplitudes within the patch.

The data values defining FDS patch ellipse **605** may be stored in memory **310**, and retrieved by ultrasound processor **305** at step **420**. Alternatively, FDS patch ellipse **605** may not exist as a predetermined set of parameters. In this case, ultrasound processor **305** may execute instructions to plot R and S values **610** (**610a** and **610b** are not yet discriminated), and then define a boundary for FDS patch ellipse **605** based on the statistical distribution of the R and S data points. This may be accomplished using known algorithms for removing outliers from data. One skilled in the art would recognize that there exist algorithms for statistically discriminating between R and S values **610a** and **610b**. Further, as used herein, the term “ellipse” may refer to a boundary of any shape.

Further, although S/R plot **600** is illustrated in FIG. **6** as a visual graph, one skilled in the art will recognize that the data need not be graphically depicted, and that the data may be stored in matrix form in memory **310**.

At step **425**, ultrasound processor **305** executes instructions to identify “bad” patches, which correspond to R and S data points **610b**. In other words, the R and S data points **610b** lie outside the FDS patch ellipse **605** and would thus not qualify as FDS. Again, this means that the signal to noise ratio and skewness are such they have a Gaussian distribution of speckle scatterers **112**, and thus the plot of correlation coefficient ρ as a function of elevation distance Δz would not conform to a Rayleigh distribution. The corresponding bad patches in first and second ultrasound images **505a** and **505b** are tagged as bad patches in memory device **310**.

At this stage of exemplary process **400**, first and second ultrasound images **505a** and **505b** are respectively divided into patches **510a/510b** and sub-patches **515a/515b**. For both images **505a** and **505b**, some of the patches **510a** and **510b** may have been tagged as bad patches, and some may have been tagged as good patches. Depending on the nature of the tissue medium, and the presence of structure such as vein and bone, it may be the case that all of patches **510a** and **510b** are tagged as bad patches. The next phase of process **400** may include identifying good and bad sub-patches among sub-patches **515a** and **515b**.

As described below, steps **430-455** are performed on sub-patches of a given bad patch of one of ultrasound images **505a** and **505b**. For convenience of description, an example scenario will be described in which the steps are performed on sub-patches **515a** of a bad patch **510a** of first ultrasound image **505a**. However, one skilled in the art will readily recognize that this description may pertain to sub-patches of **515b** of a bad patch **510b** of second ultrasound image **505b**. Further, one skilled in the art will also recognize that steps **430-455** may be performed “simultaneously” on both first and second ultrasound images **505a** and **505b** in a multi-tasking operating system or parallel processing computer architecture, and that such variations are within the scope of the invention.

At step **430**, ultrasound processor **305** executes instructions to compute the R and S values for all of the sub-patches **515a** of bad patch **510a**, using the mathematical relations shown above for computing R and S values. Ultrasound processor **305** then executes instructions to store these R and S values in memory **310**.

At step **435**, ultrasound processor **305** executes instructions to compare the R and S data values computed and at step **430** with a sub-patch FDS discrimination function. In doing so, ultrasound processor **305** maps the R and S data values on a sub-patch S/R plot.

FIG. **7** illustrates an exemplary sub-patch S/R plot **700**. Sub-patch S/R plot **700** may be similar to S/R plot **600** described above. However, sub-patch S/R plot **700** has the R

and S data values **710a** and **710b** corresponding to sub-patches **515a** (as opposed to patches **510a**), and an FDS sub-patch ellipse **705** (as opposed to FDS patch ellipse **605**). Note that the area of FDS sub-patch ellipse **705** is greater than that of FDS patch ellipse **605**. This is due to the fact that each of the sub-patches **515a** encompasses fewer speckle scatterers **112** that do the patches **510a**. Accordingly, having fewer speckle scatterers **112** means that the statistics will not be as well behaved (in a Gaussian sense) compared to having many more speckle scatterers **112**. Further, given the fact that there are fewer speckle scatterers **112** in a given sub-patch **515a**, compared to patch **510a**, the R and S data points **710a** and **710b** will generally be more broadly distributed on sub-patch S/R plot **700**, compared to R and S data points **610a** and **610b** of S/R plot **600**.

As stated above with regard to S/R plot **600**, sub-patch S/R plot **700** need not be implemented as a graphic plot, as illustrated in FIG. **7**. It may be an area of computer readable memory in which R and S data points **710a** and **710b** are mapped, along with parameter data corresponding to FDS sub-patch ellipse **705**. In doing so, the R and S data may be mapped into a 2D vector space.

Further to step **435**, ultrasound processor **305** executes instructions to discriminate R and S data points between those that lie within FDS sub-patch ellipse **705** (i.e., R and S data points **710a**) from those that lie outside FDS sub-patch ellipse **705** (i.e., R and S data points **710b**). It may do so, for example, by computing a 2D variable range space corresponding to FDS sub-patch ellipse **705**, and then comparing each R and S data point to the variable range space. FDS sub-patch ellipse **705** may exist as a set of predetermined parameter values stored in memory **310**. Alternatively, ultrasound processor **305** may execute instructions to estimate an FDS sub-patch ellipse based solely on the R and S data values, using algorithms for identifying outlier data, which are known to the art.

At step **440**, ultrasound processor **305** executes instructions to identify “bad” sub-patches, thereby also identifying all of the “good” sub-patches. Bad sub-patches are those whose R and S data points **710b** lie outside FDS sub-patch ellipse **705**. In doing so, ultrasound processor **305** may execute instructions to assign a flag, or some identifier, to the sub-patches **515a** in first ultrasound image **505a** having R and S data points **710b**.

FIG. **5C** illustrates first ultrasound image **505a**, wherein exemplary bad sub-patches **515c** exist among exemplary good sub-patches **515d**.

At step **445**, ultrasound processor **305** executes instructions to “stitch” together, or aggregate, good sub-patches **515d** of the given bad patch **510a**. In doing so, ultrasound processor **305** may, for example, execute instructions to map all of the data corresponding to speckle scatterers **112** within the good sub-patches **515d** of a given bad patch **510a**, identified at step **440** into a single array of data in memory **310**.

At step **450**, ultrasound processor **305** executes instructions to compute an R and S value for the aggregated good patch resulting from step **445**. In doing so, ultrasound processor **305** may execute instructions to compute the R and S value using the mathematical relations for these values described above.

At step **455**, ultrasound processor **305** executes instructions to compare the R and S value computed at step **450** with the FDS patch ellipse **605** (see FIG. **6**). If the R and S value lie within the FDS patch ellipse **605**, then ultrasound processor **305** assigns an identifier to the aggregated good patch. Otherwise, if the R and S value of the aggregated patch lies outside FDS patch ellipse **605**, then ultrasound processor **305** assigns an identifier to the aggregated bad patch.

Aggregating the good sub-patches **515d** into a single patch (step **445**), computing the R and S values (step **450**), and comparing the computed R and S value with FDS patch ellipse **605** (step **455**) may serve to identify false positives among the sub-patches **515a** within patch **510a**. In dividing patch **510a** into sub-patches **515a**, there is the possibility that the smaller sub-patch **515a** may completely encompass a tissue structure (e.g., vein or bone) such that the statistics within the sub-patch are well behaved. In other words, even though the sub-patch **515a** covers a structure, it does so such that the tissue volume sampled by the corresponding resolution cell is isotropic, even though it may not have any speckle scatterers **112**. In this case, the R and S value of that given sub-patch **515a** will likely lie within FDS sub-patch ellipse **705** and be identified as a good sub-patch **515d**. By recomputing the R and S value for the aggregated sub-patches **515a**, the anomalous good sub-patch **515d** will thus stand out, because the structure will be statistically revealed in the context of its multiple neighboring good sub-patches **515d**. Accordingly, if there is one or more false positives within the aggregated patch, the subsequent computed R and S data will be corrupted, thus likely placing the R and S data outside FDS patch ellipse **605**. At the conclusion of step **455**, all of the good patches and good aggregated patches may be identified in both first ultrasound image **505a** and second ultrasound image **505b**.

At step **460**, ultrasound processor **305** executes instructions to identify all good patches and good aggregated patches that are common to both first ultrasound image **505a** and second ultrasound image **515b**. In doing so, ultrasound processor **305** may store identifiers for the corresponding pairs of good patches and good aggregated patches in memory **310**. It may be the case that there are few corresponding pairs of good patches and/or good aggregated patches. In general, to determine elevation distance Δz (or out of plane motion) between first field of view **110a** and second field of view **110b**, it is desired to have at least three corresponding pairs of good patches and/or good aggregated patches.

At step **465**, ultrasound processor **305** executes instructions to compute the correlation coefficient for each corresponding pair of good patches and/or good aggregated patches between first ultrasound image **505a** and second ultrasound image **505b**. Ultrasound processor **305** may do so by computing the following relation for each pair:

$$\rho(W, Z) = \frac{\sum w_i z_i - N \mu_w \mu_z}{\sqrt{(\sum w_i^2 - N \mu_w^2)(\sum z_i^2 - N \mu_z^2)}}$$

where W and Z respectively refer to the good patch (or good aggregate patch) of first ultrasound image **505a** and the corresponding good patch (or good aggregate patch) of second ultrasound image **505b**, w_i refers to the intensity value of the i th pixel of patch W, z_i refers to the intensity value of the i th pixel of patch Z, μ_w refers to the mean intensity value for the pixels in patch W, and μ_z refers to the mean intensity value for the pixels in patch Z. Ultrasound processor **305** then stores the computed correlation coefficients $\rho(W, Z)$ in memory **310**.

At step **470**, ultrasound processor **305** executes instructions to compute an elevation distance Δz for each correlation coefficient computed at step **465**. In doing so, ultrasound processor **305** may execute instructions to retrieve a plurality of correlation curves, each corresponding to an image depth, and the correlation coefficients $\rho(W, Z)$ computed at step **465**.

FIG. **8** illustrates an exemplary ultrasound field of view **110**, and a plurality of image depths **810a-e**. For each image depth **810a-e** there is a corresponding correlation curve **805a-e**. Each correlation curve **805a-e** corresponds to a Rayleigh distribution that correlates a given correlation coefficient ρ with an elevation distance Δz , as discussed above with regard to FIG. **2**. The axial spacing of image depths **810a-e** may be substantially constant, or may vary. Further, each correlation curve **805a-e** may be stored in memory **310** as a look up table, or they may be parametrically defined. One skilled in the art will readily appreciate that such variations to the storing of correlation curves **805a-e** are possible and within the scope of the invention.

Further to step **470**, ultrasound processor **305** executes instructions to compute the elevation distance Δz from the corresponding correlation coefficients $\rho(W, Z)$. Each corresponding pair of patches (or aggregated sub-patches) W and Z has an associated image depth **810a-e**. Accordingly, the result of step **470** is a series of elevation distances Δz as a function of image depth **810a-e**.

FIGS. **9A** and **9B** illustrate two exemplary out of plane motions. FIG. **9A** illustrates a translation along elevation distance Δz ; and FIG. **9B** illustrates a rotation around the lateral or y-axis. In the former case, the elevation distance Δz computed at step **470** may be substantially constant as a function of distance. However, in the latter case, the elevation distance Δz computed at step **470** may vary in amplitude such that the location of the axis of rotation may be identified by the trend in elevation distance Δz as a function of image depth **810a-e**. Further, it will be apparent to one skilled in the art that combinations of out of plane translation and rotation are possible, and that computing elevation distance Δz as a function of image depth **810a-e** may reconstruct that motion.

At the end of process **400**, memory **310** will have stored first and second ultrasound images **505a** and **505b**, and values for the out of plane motion of ultrasound probe **100** between the acquisition of the two images. By repeating process **400** over a range of out of plane motion of ultrasound probe **100**, ultrasound processor **305** may then execute instructions to construct a 3D image of the tissue medium using image processing techniques that are known to the art.

Many variations to process **400** are possible and within the scope of the invention. For example, process **400** may be modified so that patches may be defined that encompass corresponding areas of both first ultrasound image **505a** and second ultrasound image **505b**.

FIG. **10** illustrates such a variation. As illustrated, corresponding patches **1000a** and **1000b** may be combined. To accomplish this, ultrasound processor **305** may execute instructions to combine the pixel data of patch **1000a** and **1000b** into a single array of data, and then compute the R and S data of this merged patch at step **415**. There may be two advantages in this approach. First, data from a large number of pixels (e.g., 4-5K pixels) may be obtained from a patch that is considerably smaller in each of first and second ultrasound images **505a** and **505b**. This may lead to using smaller patches, which may increase the likelihood of identifying more good patches, depending on the distribution and size of structure (e.g., vein or bone) in first and second ultrasound images **505a** and **505b**. Second, merging patches in this manner may obviate the need for step **460**, because a given merged patch is formed from corresponding areas of first and second ultrasound images **505a** and **505b**. As such, a good patch is automatically good for the same area of each image.

In another variation, ultrasound beamsteering may be employed to increase the number of pixels per patch, and thus reduce the size of each patch.

13

FIG. 11 illustrates two steered ultrasound beams **1105a** and **1105b**. A given patch **1110** may be defined in an overlap region between ultrasound beams **1105a** and **1105b**. Ultrasound beamsteering, in which the differential phasing is applied to clusters of transducers within transducer array **105**, is known to the art. By employing two steered ultrasound beams **1105a** and **1105b** to image the same patch **1110**, twice the number of pixels may be obtained from a single volume of tissue medium. This may increase the fidelity of the R and S values computed for each patch **1110**. It may also reduce the size of a given patch, which may increase the number of good patches and improve the quality of the computation of out of plane motion by having more good patches (and thus more elevation distance Δz data points). One skilled in the art will recognize that such variations to process **400** are possible and within the scope of the invention.

Further to this variation, in addition to (or alternative to) acquiring multiple images using beamsteering, process **400** may vary other ultrasound imaging parameters in imaging a single patch. For example, instead of imaging a single patch using two different beamsteered fields of view, ultrasound probe **100** may be configured to acquire multiple images of a single patch using different frequencies, or different ultrasound focusing modes that are known to the art.

FIG. 12 illustrates two ultrasound images **1205a** and **1205b**, whereby each image is acquired using different focusing modes. By using multiple frequencies and/or multiple focusing modes, more independent pixel data may be acquired for a single patch. This may increase the number of pixels for a given patch, and thus improve the statistical qualities of the later-computed R and S data, but it may also allow for a smaller patch to be used.

In another variation of process **400**, FDS patch ellipse **605** and FDS sub-patch ellipse **705** may not be implemented as hard boundaries, but may be implemented in gradations from an FDS ellipse centroid. In this case, R and S data points closer to the centroid of the FDS ellipse may be given a higher weight than those further from the centroid. In this case, the patches or sub-patches corresponding to R and S values closer to the centroid may be given a higher weight in computing out of plane motion.

The plurality of correlation curves **805a-e** may be predetermined in a calibration procedure using an isotropic tissue simulating phantom, which are known to the art. Phantom-based calibration may be done by acquiring ultrasound data of a phantom is a succession of images, each spaced apart by a controlled elevation distance Δz . Once ultrasound images are collected for a sequence of elevation distances Δz , correlation coefficients ρ may be computed for each elevation distance Δz , and then stored in a look up table in memory **310**. Alternatively, as stated above, the set of correlation coefficients ρ may also be computed and stored parametrically, to be later used at step **465** of process **400**.

An alternate, or supplemental calibration procedure may be done using a tissue sample instead of a phantom. In this case, ultrasound images may be acquired while ultrasound probe **100** is moved in a controlled fashion over a range of elevation distances Δz , similar to phantom-based calibration. Once the ultrasound image data is acquired and stored, ultrasound processor **305** may execute instructions to perform steps **405-465** of process **400**. The result is an array of correlation coefficients ρ as a function of elevation distance Δz . In this case, instead of computing elevation distance Δz , which is known, ultrasound processor **305** executes instructions to store the computed correlation coefficients ρ as a function of elevation distance Δz . Depending on the size and distribution of structure in the tissue medium, the computed correlation

14

coefficients ρ may be compared with stored correlation coefficients ρ from previous calibrations. This may be useful for verifying or refining previous calibrations.

Another variation to process **400** may include a parallel image processing path (not shown), in which a structure having a known shape may be identified in the first and second ultrasound image and used as a fiducial marker for providing additional elevation distance Δz . This additional elevation distance Δz may be used to more optimally reconstruct a 3D ultrasound image from first and second ultrasound images **505a** and **505b**. This may be useful in two exemplary scenarios: one involving an imaged surgical device, and another involving a pre-imaged anatomical structure of known shape.

FIG. 13 illustrates first and second fields of view **110a** and **110b**, along with surgical device **1305**. Surgical device **1305**, such as a needle, may be inserted into the tissue medium imaged by ultrasound probe **100**. This may be done in situations in which ultrasound imagery is used to help guide or track the surgical device. In this case, the shape of surgical device **1305** is known. Accordingly, if the reconstruction of 3D ultrasound imagery, including first and second ultrasound images **505a** and **505b**, results in a 3D image in which surgical device **1305** does not appear as it is known to appear, ultrasound processor **305** may execute instructions to further adjust the relative orientation and position of ultrasound image **505a** and **505b** so that the image of the surgical device more closely resembles its known shape. This exemplary scenario may be done in biopsy procedures, ablative therapy procedures, or other surgical procedures in which real time 3D imaging of a target tissue medium is desired. Ultrasound processor **305** may execute instructions to recognize, or segment, surgical device **1305** according to image processing algorithms that are known to the art.

FIG. 14 illustrates first and second fields of view **110a** and **110b**, and a known anatomical structure **1405**. In this exemplary scenario, the tissue medium may have been previously imaged using a 3D imaging modality, such as MRI or CT. In this case, the 3D image may include anatomical structure **1405** that will not likely have changed shape since the 3D image was acquired. In this scenario, the 3D image that is reconstructed according to the present invention (which includes ultrasound images **505a** and **505b**) may be adjusted so that the reconstructed 3D ultrasound image of anatomical structure **1405** more closely resembles that imaged previously. In either of these scenarios, ultrasound processor **305** may execute instructions according to image processing techniques that are known to the art for the purposes of manipulating 3D images to account for the configuration of fiducials common to the images.

In another variation of process **400**, ultrasound processor **305** may (once a plurality of elevation distances Δz have been computed) execute instructions to fit a plane corresponding to the plurality of elevation distances. Referring to FIGS. **9A** and **9B**, the plane to be fitted to the plurality of elevation distances Δz may be considered one of the planes illustrated. It may be the case that some of the plurality of elevation distances Δz may be statistically better than others. For example, Δz_b may be inordinately longer or shorter than the other Δz values. In this case, Δz_b would be considered an outlier, and could thus be discarded. Accordingly, process **400** may include a step whereby ultrasound processor **305** executes instructions to fit a rigid plane to the plurality of Δz values computed at step **470**, compute the errors corresponding to each Δz (i.e., the distance between each Δz and the rigid plane), and reject the Δz values that have an error greater than some threshold.

15

It will be apparent to those skilled in the art that various modifications and variations can be made in the present invention without departing from the spirit or scope of the invention. Thus, it is intended that the present invention cover the modifications and variations of this invention provided they come within the scope of the appended claims and their equivalents.

What is claimed is:

1. A method for generating 3D ultrasound imagery, comprising:

acquiring a first ultrasound image and a second ultrasound image, the first ultrasound image corresponding to a first image location, and the second ultrasound image corresponding to a second image location, and wherein the first image location and the second image location are separated by an elevation distance;

dividing the first ultrasound image and the second ultrasound image into a plurality of patches;

computing a signal to noise ratio value and a skewness value for each of the plurality of patches as statistical parameters that characterize a statistical distribution of speckle scattering within each of the plurality of patches;

comparing the signal to noise ratio value and skewness value for each patch to a range of acceptable signal to noise ratio values and a range of acceptable skewness values;

determining whether each patch of the plurality of patches is a good patch, wherein each good patch has a corresponding signal to noise ratio value and skewness value that lie within the range of acceptable signal to noise ratio values and skewness values;

computing a correlation coefficient for a corresponding pair of good patches, wherein one of the corresponding pair is from the first ultrasound image, and the other of the corresponding pair is from the second ultrasound image; and

computing an elevation distance corresponding to the correlation coefficient.

2. The method of claim 1, further comprising:

identifying a plurality of bad patches, wherein the bad patches have a corresponding signal to noise ratio value and skewness value that lie outside the range of acceptable signal to noise values and skewness values;

dividing each of the bad patches into a plurality of sub-patches; computing a sub-patch signal to noise ratio value and skewness value corresponding to each sub-patch within a bad patch;

identifying a plurality of good sub-patches, wherein the good sub-patches have a signal to noise ratio value and a skewness value that lie within a range of acceptable signal to noise and skewness values;

computing an aggregate signal to noise ratio value and skewness value corresponding to the plurality of good sub-patches;

comparing the aggregate signal to noise ratio value and skewness value to the range of acceptable signal to noise values and skewness values;

computing an aggregate correlation coefficient for corresponding pluralities of good patches between the first ultrasound image and the second ultrasound image;

computing an elevation distance corresponding to the aggregate correlation coefficient; and

constructing a 3D image using the first and second ultrasound images and the elevation distance.

3. The method of claim 1, wherein comparing the signal to noise ratio value and skewness value for each patch to a range

16

of acceptable signal to noise ratio values and a range of acceptable skewness values comprises:

mapping the signal to noise ratio value and skewness value as a data point in a 2D vector space;

mapping a Fully-Developed-Speckle ellipse in the 2D vector space; and determining if the data point lies inside the Fully-Developed-Speckle ellipse.

4. The method of claim 1, wherein comparing the signal to noise values and skewness value for each patch to a range of acceptable signal to noise ratio values and a range of acceptable skewness values comprises:

mapping the signal to noise ratio value and skewness value as a data point in a 2D vector space;

computing a distance of data point to a centroid corresponding to a Fully-Developed-Speckle ellipse; and assigning a weight value to the data point.

5. The method of claim 1, wherein computing the elevation distance comprises applying the correlation coefficient to a correlation curve.

6. The method of claim 5, wherein the correlation curve is one of a plurality of correlation curves, and wherein each of the correlation curves corresponds to a tissue depth.

7. A method for determining out of plane motion between a first ultrasound image and a second ultrasound image; comprising:

dividing the first ultrasound image into a first plurality of patches, wherein each of the first plurality of patches has a first plurality of pixel data;

dividing the second ultrasound image into a second plurality of patches, wherein each of the second plurality of patches has a second plurality of pixel data;

combining one of the first plurality of pixel data with a corresponding one of the second pixel data;

computing a signal to noise ratio value and a skewness value as statistical parameters corresponding to the combined pixel data;

comparing the signal to noise ratio value and skewness value with a range of acceptable signal to noise ratio values and skewness values;

depending on a result of the comparing, computing a correlation coefficient corresponding to the one of the first plurality of pixel data with the corresponding one of the second pixel data;

computing an elevation distance corresponding to the correlation coefficient; and

constructing a 3D image using the first ultrasound image, the second ultrasound image, and the elevation distance.

8. The method of claim 7, wherein the first ultrasound image comprises a first beamsteered image and a second beamsteered image, and wherein the first beamsteered image and the second beamsteered image have an overlapping region.

9. The method of claim 8, wherein comparing the signal to noise ratio value and a skewness value with a range of acceptable signal to noise values and skewness values comprises:

mapping the signal to noise ratio value and skewness value as a data point in a 2D vector space;

mapping a Fully-Developed-Speckle ellipse in the 2D vector space; and

determining if the data point lies inside the Fully-Developed-Speckle ellipse.

10. The method of claim 8, wherein computing the elevation distance comprises applying the correlation coefficient to a correlation curve, wherein the correlation curve is one of a plurality of correlation curves, and wherein each of the plurality of correlation curves corresponds to a tissue depth.

17

11. A system for generating 3D ultrasound images, comprising:
 an ultrasound probe;
 a processor coupled to the ultrasound probe; and
 a memory coupled to the processor,
 wherein the memory is encoded with instructions for
 acquiring a first ultrasound image and a second ultrasound image, the first ultrasound image corresponding to a first image location, and second ultrasound image corresponding to a second image location, and wherein the first image location and the second image location are separated by an elevation distance;
 dividing the first ultrasound image and the second ultrasound image into a plurality of patches;
 computing a signal to noise ratio value and a skewness value for each of the plurality of patches as statistical parameters that characterize a statistical distribution of speckle scattering within each of the plurality of patches;
 comparing the signal to noise ratio value and skewness value for each patch to a range of acceptable signal to noise ratio values and a range of acceptable skewness values;
 determining whether each patch of the plurality of patches is a good patch, wherein each good patch has a corresponding signal to noise ratio value and skewness value that lie within the range of acceptable signal to noise ratio values and skewness values;
 computing a correlation coefficient for a corresponding pair of good patches, wherein one of the corresponding pair is from the first ultrasound image, and the other of the corresponding pair is from the second ultrasound image; and
 computing an elevation distance corresponding to the correlation coefficient.

12. The system of claim 11, further comprising an optical tracking sensor disposed on the ultrasound probe and coupled to the processor.

13. The system of claim 11, wherein the memory is further encoded with instructions for identifying a plurality of bad patches, wherein the bad patches have a corresponding signal to noise ratio value and skewness value that lie outside the range of acceptable signal to noise values and skewness values; dividing each of the bad patches into a plurality of sub-patches; computing a sub-patch signal to noise ratio value and skewness value corresponding to each sub-patch within a bad patch; identifying a plurality of good sub-patches, wherein the good sub-patches have a signal to noise ratio value and a skewness value that lie within a range of acceptable signal to noise and skewness values; computing an aggregate signal to noise ratio value and skewness value corresponding to the plurality of good sub-patches; comparing the aggregate signal to noise ratio value and skewness value to the range of acceptable signal to noise values and skewness values; computing an aggregate correlation coefficient for corresponding pluralities of good patches between the first ultrasound image and the second ultrasound image; and computing an elevation distance corresponding to the aggregate correlation coefficient.

14. The system of claim 11, wherein the instructions for comparing the signal to noise ratio value and skewness value for each patch to a range of acceptable signal to noise ratio values and a range of acceptable skewness values include instructions for:
 mapping the signal to noise ratio value and skewness value as a data point in a 2D vector space;

18

mapping a Fully-Developed-Speckle ellipse in the 2D vector space; and
 determining if the data point lies inside the Fully-Developed-Speckle ellipse.

15. A system for generating 3D ultrasound images, comprising:
 an ultrasound probe; a processor coupled to the ultrasound probe; and
 a memory coupled to the processor, wherein the memory is encoded with instructions for acquiring a first ultrasound image and a second ultrasound image; dividing the first ultrasound image into a first plurality of patches, wherein each of the first plurality of patches has a first plurality of pixel data; dividing the second ultrasound image into a second plurality of patches, wherein each of the second plurality of patches has a second plurality of pixel data; combining one of the first plurality of pixel data with a corresponding one of the second pixel data; computing a signal to noise ratio value and a skewness value corresponding to the combined pixel data; comparing the signal to noise ratio value and skewness value with a range of acceptable signal to noise ratio values and skewness values; depending on a result of the comparing, computing a correlation coefficient corresponding to the one of one of the first plurality of pixel data with the corresponding one of the second pixel data; computing an elevation distance corresponding to the correlation coefficient; and constructing a 3D image using the first ultrasound image, the second ultrasound image, and the elevation distance.

16. The system of claim 15, wherein the instructions for comparing the signal to noise ratio value and a skewness value with a range of acceptable signal to noise values and skewness values includes instructions for:
 mapping the signal to noise ratio value and skewness value as a data point in a 2D vector space;
 mapping a Fully-Developed-Speckle ellipse in the 2D vector space; and
 determining if the data point lies inside the Fully-Developed-Speckle ellipse.

17. The system of claim 16, wherein the instructions for computing the elevation distance include instructions for applying the correlation coefficient to a correlation curve, wherein the correlation curve is one of a plurality of correlation curves, and wherein each of the plurality of correlation curves corresponds to a tissue depth.

18. The system of claim 15, wherein the memory is further encoded with instructions for identifying an imaged surgical device in the 3D image, comparing the imaged surgical device with a known surgical device shape, and adjusting the 3D image to conform the imaged surgical device with the known surgical device shape.

19. The system of claim 15, wherein the memory is further encoded with instructions for identifying an imaged anatomical structure in the 3D image, comparing the imaged anatomical structure with a known anatomical structure shape, and adjusting the 3D image to conform the imaged anatomical structure with the known anatomical structure shape.

20. The system of claim 15, wherein the memory is further encoded with instructions for fitting a plane to the elevation distance, computing an error corresponding to the elevation distance, and disregarding the elevation distance if the error is greater than a threshold.

* * * * *